J. Wind Eng. Ind. Aerodyn. 99 (2011) 469–482

Contents lists available at ScienceDirect

Journal of Wind Engineering and Industrial Aerodynamics

journal homepage: www.elsevier.com/locate/jweia

Numerical investigation on the three-dimensional unsteady flow past a 5:1 rectangular cylinder

Claudio Mannini [a,*], Ante Šoda [b], Günter Schewe [c]

[a] CRIACIV/Department of Civil and Environmental Engineering, University of Florence, Via S. Marta 3, 50139 Florence, Italy
[b] Faculty of Mechanical Engineering and Naval Architecture, University of Zagreb, Ivana Lucica 5, HR-10000 Zagreb, Croatia
[c] Institute of Aeroelasticity, German Aerospace Centre, Bunsenstraße 10, 37073 Göttingen, Germany

ARTICLE INFO

Article history:
Received 15 September 2010
Received in revised form
29 December 2010
Accepted 29 December 2010
Available online 5 February 2011

Keywords:
Bluff body aerodynamics
Computational fluid dynamics
Detached-Eddy Simulation
Rectangular cylinder
BARC benchmark

ABSTRACT

This paper deals with the three-dimensional simulation of the unsteady flow around a stationary 5:1 rectangular cylinder at zero-degree angle of attack, low Mach number ($M_\infty=0.1$) and high Reynolds number ($Re=26{,}400$, based on the plate thickness). Detached-Eddy Simulation (DES) was adopted as strategy of turbulence modeling. Results obtained with a hybrid mesh show satisfactory agreement when validated against experimental data and other computational results from the literature. Particular attention is devoted to the effects of the spanwise extension of the computational domain. Results show that the common choice of a spanwise period equal to the chord of the cylinder might not be enough to allow the natural loss of correlation of the pressure fluctuations and the free development of large-scale turbulent structures. The key role played by the amount of numerical dissipation, which is introduced by the second-order central difference scheme used to discretize the inviscid fluxes in the governing equations, is highlighted. The promising results obtained with DES for this benchmark test case suggest that this hybrid method is well suited for complex problems of high-Reynolds number bluff body aerodynamics and fluid–structure coupling.

© 2011 Elsevier Ltd. All rights reserved.

1. Introduction

The unsteady flow around a stationary two-dimensional rectangular cylinder with chord-to-thickness ratio $B/D=5.0$, at low Mach number ($M_\infty=0.1$), relatively high Reynolds number ($Re=26{,}400$ based on the body thickness D) and zero flow incidence ($\alpha=0^\circ$), was numerically simulated. Despite the simple geometry this is an interesting case study for the basic understanding of aerodynamics. The flow which massively separates due to the sharp leading edges, intermittently reattaches on the side surfaces of the rectangular cylinder forming unsteady turbulent separation bubbles and alternating vortex shedding. In addition, the flow field is known to develop three-dimensional structures although the cylinder geometry is two-dimensional.

This geometry has often been assumed as a reference test case for studies dealing with bridge aerodynamics and aeroelasticity (see for instance Matsumoto, 1996; Bartoli and Righi, 2006). For this reason the BARC benchmark study (Benchmark on the Aerodynamics of a Rectangular 5:1 Cylinder) was launched in July 2008 (Bartoli et al., 2008) with the aim to collect and compare a large number of experimental and numerical results on the same geometry under similar conditions obtained by different laboratories and numerical research groups. Particularly important is the fact that the clear specification of several key aspects and parameters of the experimental setup or numerical simulation is mandatory. This will allow a better interpretation of the results and understanding of the actual influence of test boundary conditions, numerical strategies and model parameters. The benchmark, to which this paper represents a contribution, should give an overview of the current capabilities and recent trends in the simulation of bluff body aerodynamics.

The simulations discussed in the current paper refer to a configuration with zero-degree angle of attack, which is the basic test case of the BARC. Nevertheless, the experiments conducted by Schewe (2006, 2009) in the high-pressure wind tunnel in Göttingen, Germany, on a stationary model highlighted the interesting case of configurations with small flow incidence, where significant Reynolds number effects can be observed. For instance, for $\alpha=2^\circ$ the lift coefficient increases of nearly 100% passing from a Reynolds number of 4000 to 120,000. Similarly, for $\alpha=4^\circ$ the increase is of about 70% with a double-bent pattern if the Reynolds number ranges from 5200 to 370,000. This last configuration was also numerically studied (Mannini et al., 2010a) solving the 2-D unsteady Reynolds-averaged Navier–Stokes (URANS) equations in combination with an explicit algebraic Reynolds stress model (EARSM). The results suggested that the progressive upstream migration of the time-averaged shear-layer

* Corresponding author. Tel.: +39 055 4796326; fax: +39 055 495333.
E-mail address: claudio.mannini@dicea.unifi.it (C. Mannini).

0167-6105/$ - see front matter © 2011 Elsevier Ltd. All rights reserved.
doi:10.1016/j.jweia.2010.12.016

reattachment location on one side of the rectangular cylinder is responsible for the strong Reynolds number effects previously mentioned. Different mechanisms of vortex shedding at low and high Reynolds numbers were highlighted too. For $\alpha=0^\circ$ Reynolds number effects in the range $5600 < Re < 370{,}000$ are less evident in terms of integral quantities: a variation as large as 15% and 5% can be observed, respectively, in the drag coefficient and in the Strouhal number (Schewe, 2009). However, it is likely that the flow field topology is more sensitive to the variation of the Reynolds number.

Along with the authors' previous URANS computations (Mannini et al., 2010a, 2008, the latter also for the case of a harmonically oscillating cylinder), other numerical simulations on the same geometry were performed by Tamura and Ito (1996), who solved the 3-D Navier–Stokes equations with a finite-difference technique for a Reynolds number of 10,000 and studied the mechanism of vortex formation for several rectangular cylinders with different chord-to-thickness ratios. Shimada and Ishihara (2002) investigated rectangular cylinders with various chord-to-thickness ratios on a 2-D domain with a two-layer k–ε turbulence model. Their computations succeeded in reproducing a smooth and periodic vortex shedding also at high Reynolds numbers, as well as the discontinuity in the Strouhal number at $B/D=2.8$ and 6.0. In contrast, the prediction of pressure and force fluctuations was significantly underestimated in some cases. In the framework of the BARC, Bruno et al. (2010) performed a 3-D Large Eddy Simulation (LES) for a Reynolds number of 40,000. They employed the proper orthogonal decomposition technique to analyze the fluctuating pressure field and concluded that, even though significant 3D flow features are apparent, the aerodynamic forces are mainly determined by the 2D modes. They also investigated in details the mechanism of vortex shedding and its relationship with the instantaneous pressure field and aerodynamic forces, highlighting the dominant contribution to the lift force of the mean pressure recovery region. Berrone et al. (2010) compared the results of a 2-D adaptive finite-element Direct Numerical Simulation (DNS) method with 2-D and 3-D finite-volume LES method at low Reynolds number (1000), obtaining close results. Then they performed 3D finite volume LES computations at higher Reynolds numbers (10,000 and 20,000).

Three-dimensional Detached-Eddy Simulation (DES) was employed in this work as an advanced strategy of turbulence modeling. This hybrid method combines the Reynolds-averaged Navier–Stokes approach near solid walls and Large Eddy Simulation away from walls, where significant amounts of turbulent kinetic energy can be economically resolved. The main aspects of the method are outlined in Section 3.2.

One of the purposes of this paper is to show the applicability of the DES technique to the rectangular–cylinder type of bluff body flows through the comparison of the results with the available experimental data. The accuracy improvement that can be obtained with respect to 2-D and 3-D unsteady RANS computations will be also highlighted. Moreover, the role played by the spanwise period of the computational domain will be investigated. In particular, it will be verified whether the common choice of a spanwise extension equal to the chord of the cylinder is reasonable by comparing the results observed in this case with those obtained by doubling the spanwise period. Finally, the sensitivity of the solution with respect to the numerical algorithms used to discretize the governing equations will be discussed. The effect of the amount of artificial dissipation introduced to stabilize the central differencing scheme for the inviscid fluxes will be the main point of the discussion.

2. Experimental results

For the geometry considered there are not many sets of experimental data available in the literature. In particular, the authors are not aware of any data about measurements of the local flow field, although Parker and Welsh (1983) gave a detailed qualitative description of the mechanism of vortex shedding on the basis of smoke visualizations.

Besides general studies on rectangular cylinders with various chord-to-thickness ratios (e.g. Okajima, 1982; Parker and Welsh, 1983; Stokes and Welsh, 1986; Knisely, 1990; Nakamura et al., 1991; Mills et al., 2002), the main experimental data considered for comparison and validation in the current work are those measured by Schewe (2006, 2009) in a high-pressure wind tunnel. In this low-turbulence closed-circuit facility (see Schewe and Larsen, 1998 for the details) the force coefficients, the Strouhal number and the mean base pressure were measured on a fixed model for a wide range of Reynolds numbers and for several angles of attack. As shown in Table 1, the measured drag C_D, normalized with respect to the body thickness D, is in good agreement with other wind-tunnel results available in the literature (Nakamura and Mizota, 1975; Matsumoto, 2005). For the Strouhal number ($St=f_sD/U_\infty$, where f_s is the dominant frequency

Table 1
Summary of the experimental results available in the literature. The spanwise aspect ratio (L/B), the blockage ratio and the longitudinal turbulence intensity (I_u) are also reported.

References	Re	L/B	Block. [%]	I_u [%]	St	C_D	C_L'
Nakamura and Mizota (1975)		4.0		0.1		~1.0	
Nakamura and Yoshimura (1982)	5500–55,000	5.0	2.0	0.1	~0.115		
Nakamura and Nakashima (1986)	4800–57,600	1.8–3.6	~1.2–2.4	0.3	~0.118		
Nakamura et al. (1991)	1000–3000	20.0	~0.2	0.3	~0.115		
Okajima et al. (1982)[a]					~0.105		
Okajima (1983)[b]	42,000		1	0.4	~0.105		
Parker and Welsh (1983)	26,600	4.1	4.92[c]	0.2	0.106		
Stokes and Welsh (1986)[d]	9800	7.6	2.54[c]	0.2	0.109		
Knisely (1990)[e]	3700	3.2	2.5	0.5	0.124		
Matsumoto et al. (2003)							
Matsumoto (2005)	40,000	3.0	3.33	0.5	0.132	~1.0	
Ricciardelli and Marra (2008)	63,600	7.3	3.75	<1	0.116		
Schewe (2006, 2009)	26,400	10.8	1.83	0.4	0.111	1.029	~0.4

[a] Reported in Nakamura and Nakashima (1986).
[b] Reported in Shimada and Ishihara (2002).
[c] Open jet section.
[d] B/D=5.2.
[e] Water channel.

of vortex shedding observed in the lift spectrum and U_∞ the free stream velocity) the experimental data are more scattered.

The pressure coefficient distribution at zero-degree angle of attack for two different Reynolds numbers was measured by Matsumoto (2005) in the Kyoto University wind tunnel, Japan. Finally, the pressure measurements performed in the CRIACIV wind tunnel in Prato, Italy (Galli, 2005; Ricciardelli and Marra, 2008) are also referred to.

Given the lack of local flow measurements for this geometry, a qualitative reference are the results obtained by Mizota and Okajima (reported in Shimada and Ishihara, 2002) for a slightly bluffer 4:1 rectangular cylinder, that is supposed to generate a flow field similar to that of the geometry considered.

3. Numerical methods

3.1. The flow solver

The numerical simulations were performed using the finite-volume unstructured solver DLR-Tau code (Gerhold et al., 1997; Schwamborn et al., 1999; Haase et al., 2006), developed by the German Aerospace Centre (DLR). The code solves the compressible Navier–Stokes equations using vertex-centered metrics with second-order spatial and temporal accuracy. Viscous terms are treated using a conventional second-order central differencing scheme. In the current work the inviscid fluxes are approximated using a central difference scheme stabilized with artificial dissipation, as explained in details later on.

The advancing in time is performed through the dual time-stepping approach. The time derivatives are first discretized with a second-order backward difference formula and the resulting sequence of nonlinear steady-state problems is solved in pseudo-physical time by an explicit three-stage Runge–Kutta scheme, until a steady solution in pseudo-time is reached. The local convergence within each physical time increment is accelerated by means of the local time-step technique, where the largest time step compatible with the Courant–Friedrichs–Lewy criterion is chosen cell by cell for each inner iteration. As a consequence, no physical meaning can be attributed to the transient to the local steady state. Explicit smoothing of the residuals and multigrid algorithms are also adopted.

3.2. Detached-eddy simulation

An economical strategy to approach turbulent flows is to solve the unsteady RANS equations in combination with additional equations for turbulence modeling. Nevertheless, in spite of their computational efficiency, turbulence models, especially if based on the linear Boussinesq eddy-viscosity hypothesis, are unable to capture complex interaction mechanisms between Reynolds stresses and mean velocity field in case of the strong streamline curvature, which characterizes the flow past bluff bodies (Shur et al., 1999; Travin et al., 1999; Spalart, 2000; Lübcke et al., 2001; Wilcox, 2006). The 2-D URANS approach was recently explored by the authors for the 5:1 rectangular cylinder (Mannini et al., 2010a) and for a bridge section (Mannini et al., 2010b) and some interesting results were obtained in combination with an explicit algebraic Reynolds stress model. Nevertheless, limited accuracy for these complex flows was apparent.

A better alternative to the unsteady RANS approach for the simulation of problems with massively separated flow is to use the Large Eddy Simulation (LES) approach. However, LES requires three-dimensional grids and wall-resolved LES (WRLES) becomes unaffordable when high-Reynolds-number thin turbulent boundary layers have to be resolved due to the necessary grid refinement, as the costs are of the order of a poorly resolved Direct Numerical Simulation (Spalart et al., 1997). Wall-modeled LES (WMLES) reduces the computational requirements at high Reynolds numbers, but the decision about the location of the interface between LES and modeled flow regions is highly critical for the success of a zonal WMLES.

In order to overcome these difficulties the non-zonal Detached-Eddy Simulation (DES) method was introduced in Spalart et al. (1997) and Shur et al. (1999). DES is a hybrid RANS–LES method and the switching between the RANS and LES modes is controlled by the characteristic turbulent length scale l_t, which for the Spalart–Allmaras variant (SA-DES) used in this work is defined according to the following blending function:

$$l_t = \min\{d, C_{DES}\Delta\}, \quad \Delta = \max\{\Delta_x, \Delta_y, \Delta_z\} \tag{1,2}$$

where d denotes the distance from the wall and Δ the largest edge length of the local grid cell. Near the wall, where a well-resolved LES is unaffordable or too expensive, $l_t = d$ and therefore the RANS mode of the DES model is active, i.e., the additional equation works as an eddy-viscosity model (Spalart and Allmaras, 1992). Away from walls, where turbulent kinetic energy can be economically resolved, $l_t = C_{DES}\Delta$ and, under an equilibrium assumption, the turbulence model reduces to a Smagorinsky sub-grid scale model. The additional parameter with respect to pure URANS simulations is the constant C_{DES}. Shur et al. (1999) calibrated this parameter against decaying homogeneous isotropic turbulence (DHIT) to ensure that the LES mode returns a proper turbulent kinetic energy cascade (i.e., the Kolmogorov 5/3's law is resolved). $C_{DES} = 0.65$ is the recommended value, obtained by adopting a centered fourth-order accurate differencing scheme. A smaller value of the DES constant can be used for more dissipative codes (Spalart, 2001; Strelets, 2001; Šoda, 2006). However, the optimal choice of C_{DES} is closely tied into the numerical properties of the numerical scheme adopted. Spalart (2001) claims that DES is not very sensitive to this parameter. In the present work $C_{DES} = 0.45$ and 0.65 are assumed according to the numerical diffusion of the second-order central-difference scheme employed, on the basis of the calibration using DHIT (Weinman et al., 2006).

With this approach 3-D meshes are needed and, while the number of grid points required for a properly designed DES mesh is not much higher than that for a URANS mesh, the requirement to adopt smaller time steps and the need to obtain a reasonable statistical convergence of the solution have limited the use of DES within industry. For the present geometry, due to the presence of sharp edges and the absence of thin turbulent boundary layers, a pure LES method might give fair results with the same level of refinement of the spatial discretization. Therefore, it would be extremely interesting to compare the DES and LES results obtained with the same computational mesh and discretization algorithms.

Spalart et al. (2006) proposed the Delayed Detached-Eddy Simulation approach (DDES), a modified version of DES where a blending function depending on the computed flow quantities (velocity gradients and eddy viscosity) is introduced in order to maintain full RANS behavior in case of thick boundary layers and ambiguous grids (i.e., grids with small streamwise spacing with respect to the boundary layer thickness but not small enough to sustain LES), thus avoiding premature grid-induced separation due to modeled stress depletion. In this formulation of DES a low-Reynolds number correction is also introduced in order to compensate the activation of the low-Reynolds number terms in the RANS equation when acting as a sub-grid scale model in the LES mode.

A wide range of DES computations using structured grids are reported in Strelets (2001), whereas the first application of this technique with a second-order accurate unstructured code and hybrid grids can be found in Hansen and Forsythe (2003). Travin

et al. (1999) showed that reasonable results with the DES approach can be obtained only in combination with three-dimensional meshes.

3.3. Artificial dissipation

The choice of the numerical scheme for the discretization of the inviscid fluxes of the Navier–Stokes equations is a key issue in LES and therefore also in DES. If the truncation errors introduced by the discretization overwhelm the sub-grid scale model dissipative terms, the simulation behaves more as a Monotonic Integrated Large Eddy Simulation (MILES) than as a proper LES. For this reason the use of higher-order schemes is recommended (Kravchenko and Moin, 1997; Ducros et al., 2000).

In order to keep the numerical diffusion as low as possible, which is always an issue with unstructured CFD codes, the inviscid fluxes are discretized with a central difference scheme, which is second-order accurate for sufficiently smooth meshes. Nevertheless, crude central differencing is not stable and spurious oscillations can easily appear in the solution. Therefore an artificial dissipation model is required to stabilize the scheme. Jameson et al. (1981) proposed an algorithm based on a blend of second and fourth differences. A fourth difference helps to damp out the high-frequency modes in smooth regions of the flow solution (background dissipation), whereas a nonlinear second difference limits the oscillations in the neighborhood of regions with large gradients, such as shocks, by reducing the accuracy of the discretization to first order. A nonlinear shock detector, proportional to an undivided Laplacian of the pressure, preserves the second-order accuracy of the scheme in smooth regions.

In the original version of the algorithm (scalar dissipation) the dissipation is scaled through a coefficient based on the spectral radius of the Jacobian matrix of the inviscid fluxes. Second- and fourth-order artificial dissipation can be independently re-scaled by means of two user-prescribed constants. The coefficient k_2 multiplying the second-order dissipation term is not critical in subsonic flows and it should be set to an as low as possible value; with $k_2=0.0$ usually chosen as a reasonable option. In contrast, the choice of the coefficient of the fourth-order dissipation term, k_4, is more crucial as it will be shown in Section 5.3. Originally Jameson et al. (1981) and Mavriplis et al. (1989) recommended $k_4=1/256$. In contrast, Swanson and Turkel (1992) suggested to adopt a value between 1/64 and 1/32.

An advantage of the artificial dissipation approach is that it allows the user to control the amounts of dissipation introduced in the numerical solution. Nevertheless, the previously mentioned scalar scaling can add too much artificial viscosity to slower waves. A matrix dissipation scheme was therefore proposed (Turkel, 1988; Swanson and Turkel, 1992). In this approach the scaling of the dissipation is not obtained by means of the spectral radius of the Jacobian of the inviscid fluxes but with a matrix related through a similarity transformation to the absolute values of the eigenvalues of the flux Jacobian, with a limiter proportional to the spectral radius of it, in order to avoid zero entries near stagnation points or sonic lines. This method gives an appropriate viscosity for each equation yielding a global reduction of the numerical dissipation with respect to the scalar approach. Swanson and Turkel (1992) also discussed the conditions under which the scheme satisfies the total variation diminishing property.

In the Tau code the central difference scheme with artificial dissipation is implemented following the strategy described in Mavriplis et al. (1989) for unstructured and highly stretched cells. The dissipation terms are frozen after the first Runge–Kutta stage and they are not applied to the turbulent equation. Specific tests on decaying homogeneous isotropic turbulence (discussed in Mannini et al., 2009) demonstrated that the scalar dissipation model tends to damp out the high wavenumber components of turbulence which could be resolved with properly designed DES or LES grids. Conversely, significant improvement can be obtained with the matrix dissipation form of the central difference algorithm.

Kravchenko and Moin (1997) highlighted the important role played by the aliasing errors in the LES approach and demonstrated how the discretization of the skew-symmetric form of the inviscid fluxes of the Navier–Stokes equations minimizes these errors. In this case, however, it is important to check that the equation residuals are small and the continuity equation is sufficiently well satisfied in order to ensure that the skew-symmetric operator performs correctly as an energy-conserving operator. This can require an increase in the number of inner iterations and/or a reduction of the CFL number in the dual time-stepping algorithm. However, the second-order schemes are supposed to be less sensitive to aliasing errors than higher-order schemes, as truncation errors are much larger. In Section 5.3 the comparison between the solutions obtained by discretizing the skew-symmetric and the usual divergence form of the inviscid fluxes will be discussed.

4. Spatial and temporal discretization

In this work hybrid meshes are employed, characterized by structured quadrilateral cells around the body profile, in order to better capture the large viscous effects, and unstructured triangular cells in the remaining part of the domain. The use of hybrid grids presents several drawbacks: the discretization of the flow fluxes in the unstructured domain is more diffusive than in the structured domain, and usually a finer spatial discretization is necessary to obtain grid-independent results. In addition, it is complicated to obtain stable algorithms with order of accuracy higher than second for the unstructured discretization of gradients. Another disadvantage of hybrid grids is the fact that standard methods of grid-convergence study, such as Richardson extrapolation, are very difficult to employ rigorously. Nevertheless, unstructured grids allow much easier and faster meshing of complex geometries, as well as convenient and economic mesh refinements just where it is needed. For these reasons their use has become increasingly popular both in research and industrial applications. Despite the fact that, due to the simplicity of the geometry, structured or even Cartesian grids would have been more appropriate for the present test case, the use of hybrid meshes was preferred for ease of wake refinement and as an exploring study for more complex bluff body geometries.

Fig. 1 shows the 3-D grid (1,703,585 nodes and 2,957,440 cells) obtained by extruding a 2-D grid for one-chord length in the spanwise z-direction ($L/B=1.0$), using 65 nodes to discretize the resulting edges ($\Delta z/B=1/64$). Therefore the mesh is structured and equidistant in the spanwise direction. The second grid used is identical to the first one but presents a double spanwise period ($L/B=2.0$) and the same z-spacing (3,380,961 nodes and 5,914,880 cells).

The height of the first structured layer is chosen in order to have maximum wall-unit values in the normal direction $y+\approx 1$ ($\Delta y_1/B=5.0\times 10^{-5}$). The near-wall part of the mesh consists of 28 prismatic layers with a stretching factor in the wall normal direction $\Delta y_{j+1}/\Delta y_j=1.23$, for a total height of $0.353D$. It is worth noting that Spalart (2001) observed that in DES applications very little is typically gained by going below $y^+=1$ and $\Delta y_{j+1}/\Delta y_j=1.2$. In the streamwise and spanwise directions the spacing is such that the maximum $x+\approx z+\approx 300$, with significant refinement in the neighborhood of the sharp edges.

Isotropic cells with dimension equal to $B/64$ are designed in the so-called "focus region" (Spalart, 2001), where the largest geometry-dependent turbulence structures are generated, which

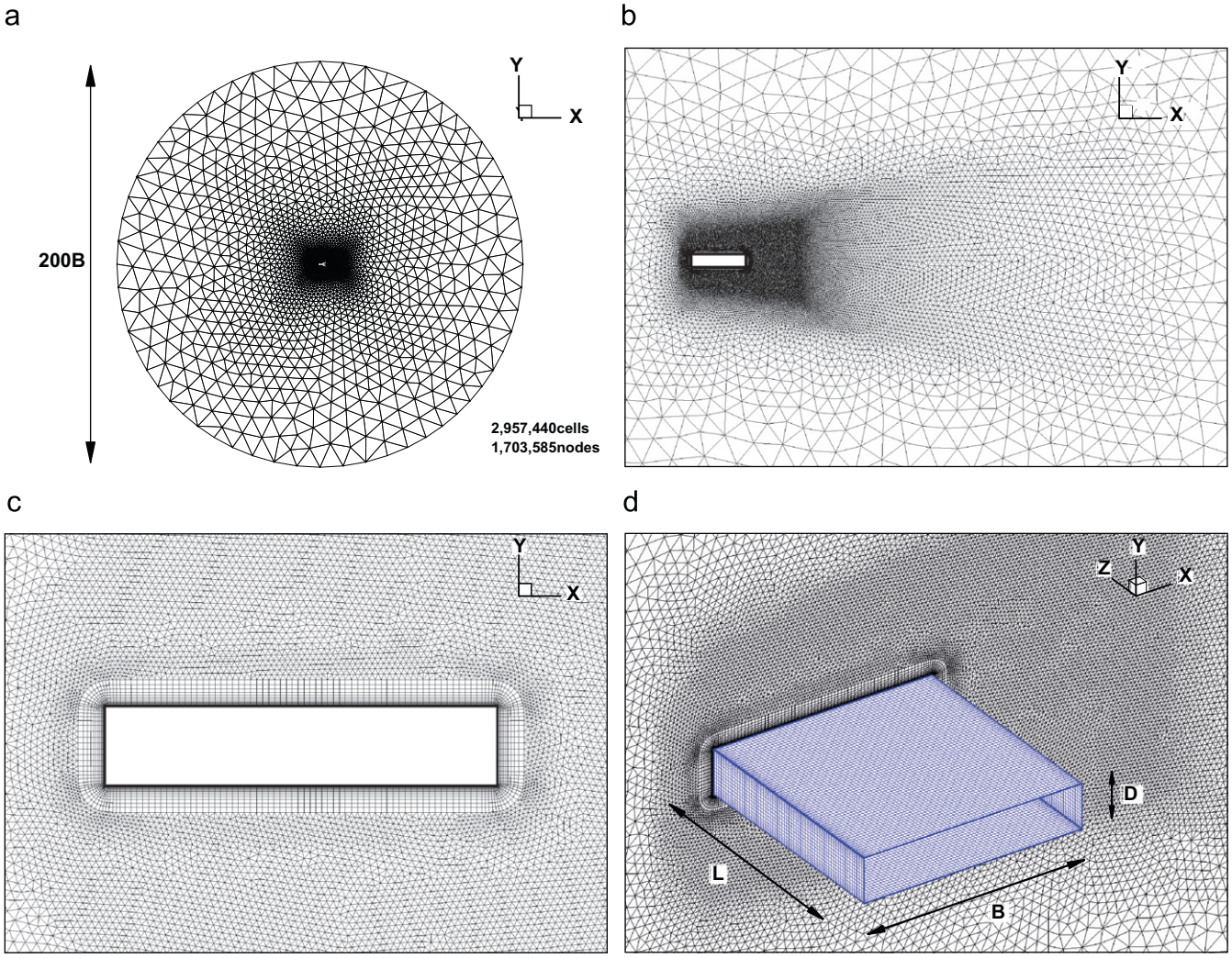

Fig. 1. Three-dimensional mesh used in the computations ($L/B=1.0$).

represents the optimal conformation for the LES mode of DES. In fact, the premise of a well resolved LES is to filter out only eddies that are small enough to be products of the energy cascade, and therefore statistically isotropic (Spalart, 2001). Consequently, in this physically correct condition for LES, refinement in just one or two directions is a waste of resources. The extension of the assumed focus region is shown in the top-right frame of Fig. 1 (one chord downstream of the rectangular cylinder). The grid spacing is smoothly enlarged when going into the supposed "departure region" and becomes very coarse in the "Euler region" (according once again to the terminology followed by Spalart (2001)).

The nondimensional time-step size is $\Delta t^*=0.017$, where $t^*=tU_\infty/D$ is the number of traveled lengths D by a fluid particle in a time unit ($U_\infty=34.0$ m/s is the free stream velocity), in order to discretize the expected period of vortex shedding with more than 500 time steps. This temporal discretization is finer than the one suggested by Spalart (2001) on the basis of the cell size in the focus region.

The choice of the resolution of the spatial and temporal discretization relies on literature results but it is also based on the indications offered by the URANS grid-convergence study presented in Mannini et al. (2010a) and by the preliminary DES computations discussed in Mannini et al. (2007). It is also worth noting that rigorous grid-convergence studies for DES simulations are not only burdensome but also particularly problematic (Weinman et al., 2006) and they were not attempted in this work.

The governing equations are solved on a cylindrical computational domain with a radius equal to $100B$ (top-left frame of Fig. 1). The farfield boundary condition is placed at the external contour of the domain, i.e., free stream values of the flow variables are assigned as external values and the values at the boundary are calculated employing the theory of Whitfield and Janus (1984). The calculation of the fluxes crossing the boundary faces is done using the AUSM Riemann solver. No-slip and periodic boundary conditions are imposed, respectively, at the body surface and at the lateral planes of the computational domain. The turbulence model is activated everywhere by prescribing at the farfield boundary small values of the turbulent viscosity (10% of the laminar viscosity). Nevertheless, no resolved turbulence is generated upstream of the rectangular cylinder, so that the simulations are performed with an ideal smooth free stream. As initial condition, free stream values of the flow variables are imposed at all grid nodes, unless the computation is restarted from the flow field resulting from a previous simulation.

5. Discussion of the results

5.1. Comparison with URANS solutions

The first DES simulation considered was performed on the grid with a spanwise period equal to the chord length of the cylinder

($L/B=1.0$). The basic version of DES was adopted (Spalart et al., 1997; Shur et al., 1999), scalar dissipation was employed to stabilize the central difference discretization of the inviscid fluxes and a value of the constant $C_{DES}=0.45$ was assumed. 100 inner iterations were performed for each physical time step. With the designed grid and the chosen value of the DES constant, the LES mode was active in the 86% of the computational volumes.

In Mannini et al. (2008, 2010a) the results of this 3-D simulation were compared to those of 2-D URANS computations obtained with the eddy-viscosity one-equation turbulence model of Spalart and Allmaras (1992) (see also Edwards and Chandra, 1996) and an EARSM model, namely the Linearized Explicit Algebraic (LEA) model (Rung et al., 1999), closed with the k–ω equations of Wilcox (1988). Despite the fact that the Spalart–Allmaras model represents the additional equation for the DES approach employed in the current study, the URANS solution with this eddy-viscosity model was steady (Table 2). A significant improvement of the result is given by the 2-D URANS-LEA solution. In contrast, no large difference can be observed between the 2-D and 3-D solutions (apart from a significant increase in the drag standard deviation) as the flow field resolved by the URANS equations contains only limited three-dimensional flow features (Mannini et al., 2010a). This result is not surprising as it was noted in Shur et al. (2005) that 3-D URANS simulations must be conducted using significantly larger spanwise periods than those necessary to develop three-dimensionality in DES or LES. Also, the result seems to be very sensitive to the spanwise extension of the computational domain and turbulence model chosen, so that the authors claim that 3-D URANS computations can be effective in order to better predict the mean drag coefficient but are often not very beneficial where transient flow characteristics are concerned (Shur et al., 2005). In addition, in many cases three-dimensionality has to be triggered by introducing a random perturbation in the initial condition. In one test case discussed in Shur et al. (2005) 3-D structures could be sustained only by restarting from a DES flow field.

Fig. 2 compares the lift and drag time histories computed with the 3-D URANS-LEA and 3-D SA-DES equations. Both force coefficients are normalized with respect to the body thickness D. It is evident that the result of the URANS-LEA simulation is nearly periodic (apart from the initial transient, until $t^*\approx 180$, which has no physical meaning and has to be discarded), whereas significant stochastic behavior characterizes the other simulation due to the LES mode of DES. This fact allows to consider much shorter computations in the case of the URANS approach. It is also worth noting that 2-D URANS results were periodic (although very small stochastic content can appear in case of very fine grids, as noted in Mannini et al., 2010a) and therefore the stochastic behavior is due to 3-D flow features that, as previously noted, are limited in the 3-D URANS simulation considered.

In Table 2 the mean and standard-deviation values of the force coefficients and the Strouhal numbers are compared with the experimental results of Schewe (2006, 2009). The non-negligible mean lift values are probably due to the limited length of the computations which does not allow a proper average over the phenomena at much lower frequency than that of vortex shedding. In addition, 2D URANS results demonstrate that part of this mean lift value is a numerical artefact that needs very long simulations to disappear. A precise reference experimental value for the standard deviation of the force coefficients is difficult to be assessed since several phenomena can strongly influence it. In particular, due to the high air density in the high-pressure wind tunnel, i.e., low Scruton number, sub- or super-harmonic resonances with the vortex shedding can induce the vibration of the model, though nominally stationary, and therefore increase the amplitude of the fluctuations, especially when the natural frequency of the model is not very high (slightly less than 100 Hz in Schewe's experiments). As standard deviation of the lift coefficient, $C_L'=0.4$ seemed to be a reasonable reference value (Schewe, 2006, 2009). Tamura and Ito (1996) obtained $C_L'\approx 0.15$ Shimada and Ishihara (2002), a value of about 0.05 and Bruno et al. (2010) $C_L'\approx 0.75$. It can be remarked that the URANS-LEA simulation slightly underestimates the Strouhal number, whilst C_L' is

Table 2
Comparison with experiments of Strouhal number and mean (C_D, C_L) and standard-deviation (C_D', C_L') values of drag and lift coefficients. t^*_{INT} denotes the nondimensional time units considered for the calculation of the statistics.

	St	C_L	C_D	C_L'	C_D'	t^*_{INT}
2-D URANS-SA	–	0.008	0.968	–	–	–
2-D URANS-LEA	0.094	0.032	1.060	1.075	0.019	74.2
3-D URANS-LEA (L/B=1.0)	0.095	0.013	1.071	1.035	0.029	84.5
3-D SA-DES (L/B=1.0)	0.103	0.047	1.016	0.553	0.055	464.5
3-D SA-DES (L/B=2.0)	0.102	0.005	1.029	0.421	0.043	715.0
Experiments (Schewe, 2009)	0.111	0.0	1.029	~0.4		

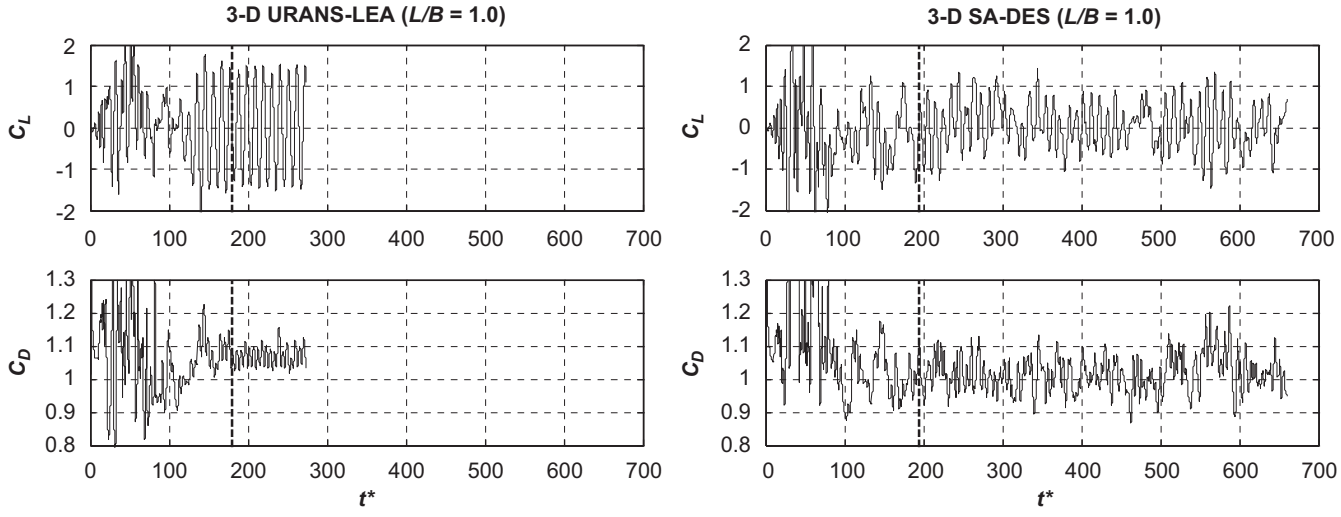

Fig. 2. Lift and drag coefficient time histories computed with the 3-D URANS-LEA and SA-DES approaches. The dashed vertical lines indicate the nondimensional time instants after which the signals are considered to calculate the results reported in Table 2.

significantly overpredicted due to the nearly two-dimensional flow field computed. A significant improvement can be obtained by applying DES, especially in terms of standard-deviation value of the lift coefficient, which is reduced by almost 50%. Nevertheless Strouhal number still seems to be underestimated by about 7%.

Fig. 3 shows the mean and standard-deviation values of the pressure coefficient on the body surface with several wind tunnel test results reported for comparison. The mean pressure coefficients of both URANS-LEA and SA-DES computations, that are also spanwise-averaged, are in good agreement with experiments, which are characterized by limited scatter. Slightly lower values of the mean base pressure are predicted by the DES computation with respect to the URANS one. In contrast, as observed also for other bluff body flows, the wind tunnel data for the standard deviation of the pressure coefficients present a significant dispersion. This is probably due to the fact that the distribution of C_p' is more sensitive to the experimental boundary conditions than the mean values of pressures. In particular, the measurements of Matsumoto (2005) suggest a significant dependence on the Reynolds number. For similar reasons also the numerical results for C_p' are in worse agreement than those for the mean values of C_p. However all the simulations predict nearly the same position of the peak of the pressure fluctuations, at a streamwise position $x/D \approx 1.1$ ($\xi/D \approx 4.1$ in the figure), where $x=0$ denotes the center of the rectangular cylinder, in agreement with the experiments. Nevertheless, with respect to the wind tunnel data (and also to URANS-LEA results) the SA-DES computation underestimates the magnitude of the peak. In contrast, in the range $0.5 < \xi/D < 3.5$ the numerical results fall between Matsumoto's values for $Re=20{,}000$ and 40,000. In addition, the URANS-LEA and SA-DES computations predict the same values of C_p' immediately after the leading edge for a distance of about D; then, for a length of about $1.5D$ the fluctuating pressures computed with DES are larger than those obtained with the URANS equations. The opposite condition is observed around the aforementioned peak of C_p', where the URANS-LEA results are in better agreement with the experiments of Matsumoto (2005). Finally, near the trailing edge and in the base region, the DES fluctuations are again larger. The experimental results of Galli (2005) for C_p' are surprisingly large, also in the stagnation face, and that might be due partly to the free stream wind tunnel turbulence.

In Fig. 4 the DES time-averaged flow field is depicted showing that the shear-layer mean reattachment occurs near the downstream vertices of the rectangular section, at $x/D=2.25$, in agreement with the computational results of Bruno et al. (2010), who

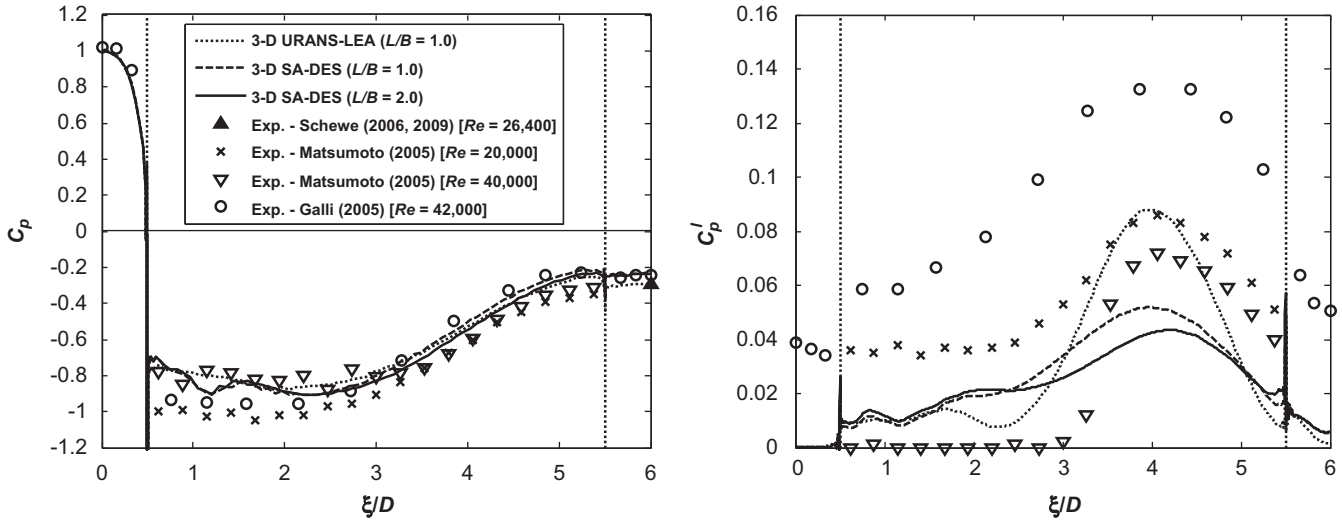

Fig. 3. Comparison with experiments of the mean (left) and standard-deviation values (right) of the computed pressure coefficient distribution. $\xi/D=0$ and 6 denote, respectively, the stagnation and the base body contour points. The statistics for the three numerical simulations are calculated, respectively, over 230, 2633 and 2668 data sampled every $10\Delta t^*=0.17$.

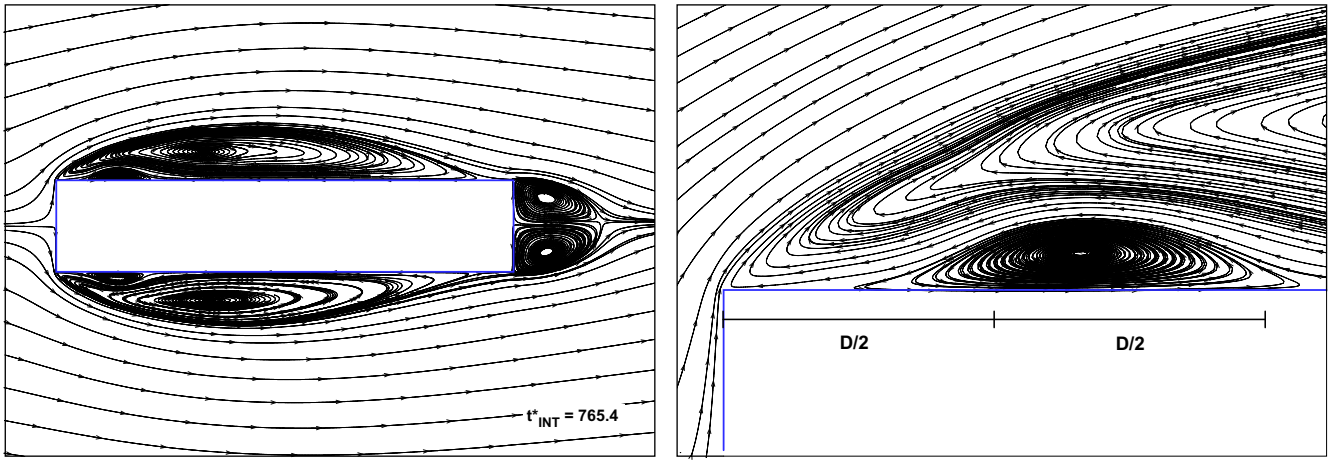

Fig. 4. Streamlines of the time-averaged flow field. A close-up view near the upstream top edge is reported in the right frame.

found $x/D=2.165$. Matsumoto et al. (2003) deduced from the distribution of mean and standard-deviation values of pressure that the reattachment point should be located at a distance of about $7B/8$ from the leading edge, i.e., at $x/D\approx 1.875$. Also the length of the recirculation region behind the body well agrees with the LES result of Bruno et al. (2010), the time-averaged saddle point being located at $x/D=3.47$. A nearly steady counter-rotating secondary vortex embedded in the main unsteady bubble is resolved close to the leading edge (Fig. 4), in agreement with the measurements of Crompton (2001) for a flat plate at shallow incidence. The latter was also numerically simulated in Collie et al. (2008) and the secondary bubble was not predicted by both Wilcox k–ω and Menter-SST models while it was obtained with LES. The secondary vortex is also evident in the LES simulation of Bruno et al. (2010) but in that case it looks longer and thinner. In the URANS-LEA results described in Mannini et al. (2010a) this counter-rotating vortex is present but much smaller. In addition, the center of the time-averaged main bubbles was found significantly downstream with respect to the present position.

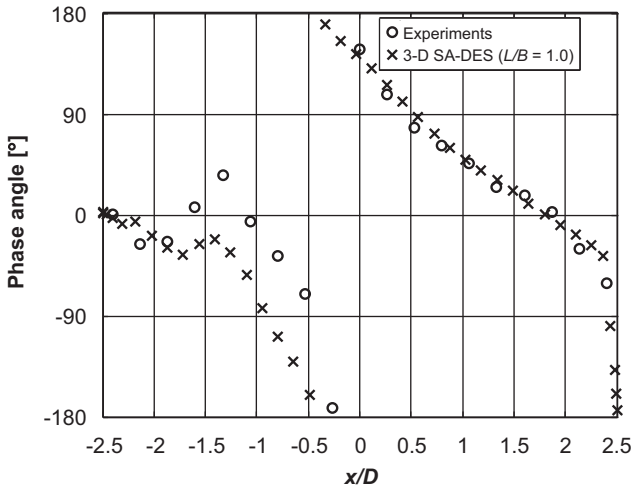

Fig. 5. Phase angle of the fluctuating pressure coefficient component corresponding to the Strouhal frequency at different streamwise positions with respect to the leading edge (1016 data sampled every $10\Delta t^*=0.17$). Experimental data from Ricciardelli and Marra (2008) refer to a Reynolds number of 63,600.

Finally, in Fig. 5 the phase angle of the pressure coefficient fluctuations at the dominant frequency of vortex shedding, relative to that of the leading edge, is plotted along the side face of the cylinder. The wavelength of the C_p fluctuations is approximately equal to the body chord, i.e., just one vortex travels at a time along the cylinder surface. This result is in agreement not only with the experimental data of Ricciardelli and Marra (2008) but also with the measurements of Nakamura et al. (1991), who interestingly showed that the vortices become two for $B/D=6.0$. However, lower phase angles with respect to the experiments can be observed in the first half of the cylinder. In particular, it is worth noting that in the neighborhood of the previously mentioned counter-rotating secondary vortex the phase angles are negative, whereas in the experiments they are positive, suggesting that the flow topology in this region may be different.

5.2. Influence of the spanwise period

A computation with the same parameters discussed in the previous section was repeated on the grid with double spanwise period ($L/B=2.0$). The computed force coefficients are shown in Fig. 6 (left frame). Low-frequency modulations in the lift coefficient time history are apparent. The Strouhal number as well as the mean and standard-deviation values of lift and drag coefficients are reported in Table 2 and their trend with respect to the length of the computation is highlighted in the right frame of Fig. 6. It can be remarked that more than 900 nondimensional time units are necessary to obtain reasonably stable values of the second-order statistical moments and a mean value of the lift coefficient satisfactorily close to zero. Even longer signals are needed to obtain stable higher-order moments, making these computations extremely expensive (see also Travin et al., 1999). By doubling the spanwise extension of the computational domain no significant changes are observed for the Strouhal number and the mean drag, while the fluctuations of the force coefficients significantly decrease. In contrast, the mean and standard-deviation values of the pressure distribution do not change appreciably (Fig. 3).

In order to better investigate the effect of the spanwise extension of the computational domain, the correlation coefficient of the pressure fluctuations at two different chordwise locations ($x/D=\pm 1.6$) as a function of the spanwise distance Δz

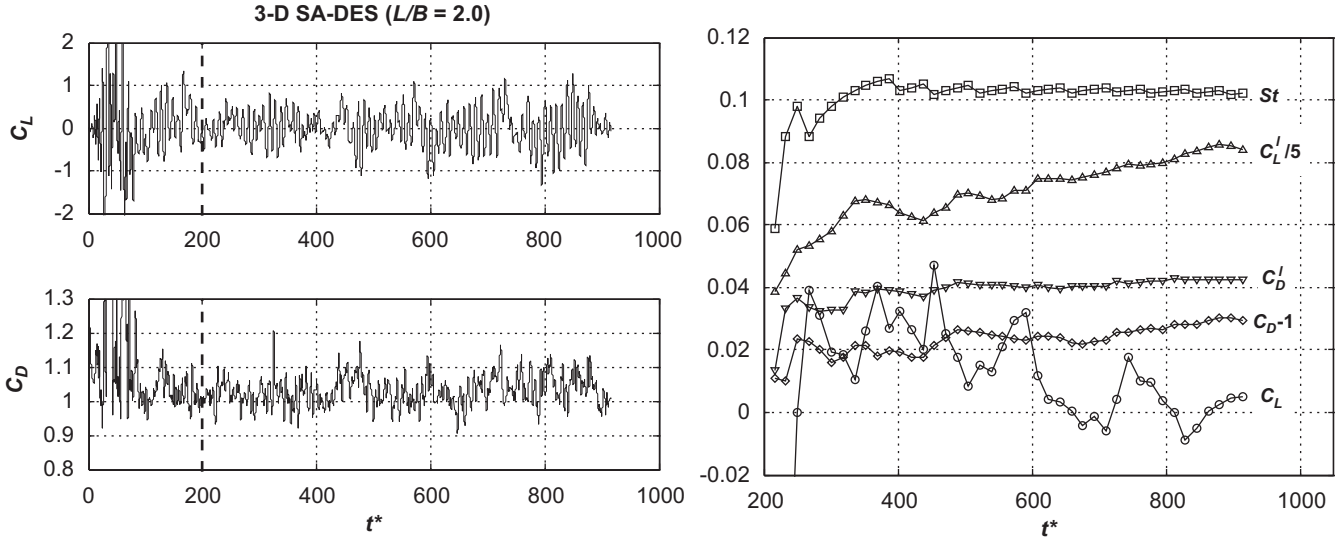

Fig. 6. Lift and drag coefficient time histories for the computation with two-chord spanwise period (left) and pattern of convergence of Strouhal number and mean and standard-deviation values of the force coefficients (right). The dashed vertical line on the left indicates the nondimensional time instant after which the signals are considered to calculate the results reported in Table 2.

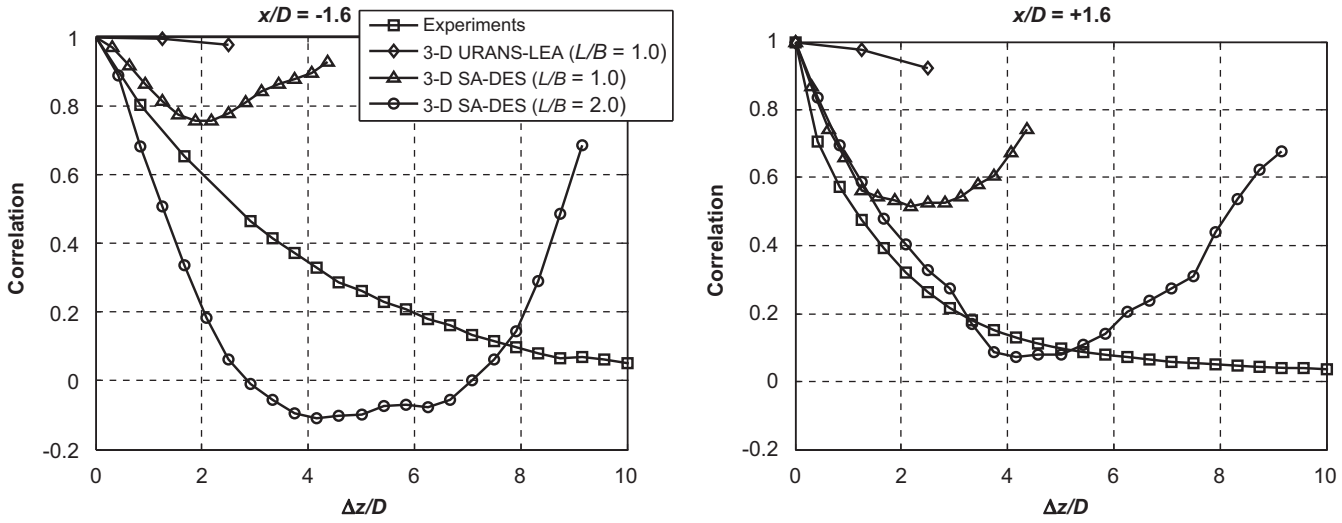

Fig. 7. Spanwise correlation of the pressure coefficients corresponding to an upstream ($x/D=-1.6$) and a downstream location ($x/D=1.6$). The correlation coefficient for the three numerical simulations is calculated, respectively, over 230, 2500 and 2668 data sampled every $10\Delta t^*=0.17$. Experimental data from Ricciardelli and Marra (2008) refer to a Reynolds number of 63,600.

is shown in Fig. 7. The results suggest that the common choice of a distance between the periodic boundary planes equal to the chord of the cylinder is not enough in this case to allow the natural loss of correlation of pressures and the free development of large-scale turbulent structures. In fact, correlation first decreases with the spanwise distance, reaches a minimum and then starts to increase again. This nearly symmetric U-shaped pattern is due to the effect of periodic boundary conditions (see also O'Neill et al., 2004). As a consequence, the standard deviation of integral force coefficients might be overestimated. If a two-chord spanwise length of the cylinder is adopted, one observes a remarkable decrease of the pressure correlation, which corresponds to a reduction of lift and drag standard deviations of more than 20%. Nevertheless, the effect of periodic boundary conditions imposed at the lateral planes is still non-negligible and an even larger spanwise period may be required. In particular, Fig. 7 shows that, considering an array of pressures in the downstream half portion of the cylinder ($x/D=1.6$), the correlation coefficient for the case $L/B=2.0$ is close to that obtained from measurements. In addition, for spanwise distances $\Delta z/D<1.5$ correlations for one-chord and two-chord spanwise periods are identical. Conversely, the results for the upstream array ($x/D=-1.6$) clearly overestimate or underestimate the experimental data, respectively, for $L/B=1.0$ and 2.0. Furthermore, the results of the two simulations are different also for very small spanwise distances. It is also worth noting that in the last case negative correlation is obtained for about $3<\Delta z/D<7$. According to the numerical results (in agreement with Matsumoto's pressure measurements at $Re=40{,}000$, as shown in Fig. 3) the flow field is nearly steady with small pressure fluctuations at this chordwise location $x/D=-1.6$, characterized by the presence of the secondary counter-rotating vortex (Fig. 4). A discrepancy with experiments in this region was already apparent from the comparison in Fig. 5. After time-averaging the flow field three-dimensional structures, probably related to very low-frequency phenomena, can still be found in this region. The negative correlation observed in the numerical results may partly be due to these nearly steady three-dimensional structures as their spanwise wavelength is compatible with the correlation pattern shown in Fig. 7.

Results for the 3-D URANS-LEA simulation are also reported in Fig.7 for the sake of comparison. The large values of the correlation coefficient well agree with the fact that the computed flow field is characterized by limited three-dimensional features.

According to Ricciardelli (2010) the correlation length of the lift force is not much smaller than the cylinder chord ($L_i/D=4.3$), nevertheless the effect of periodic boundary conditions implies that a spanwise extension of the computational domain even larger than $2B$, that is $10D$, might be needed in order to allow the free development of the three-dimensional wake of the cylinder. It is also worth mentioning that in wind tunnel experiments, in order to limit the end effects, an aspect ratio $L/B=3$ is considered as the minimum for a two-dimensional model of a moderately bluff cylinder, though ratios of 5 or 6 are preferable. Conversely, for very bluff bodies much higher aspect ratios are required.

Fig. 8 shows the coherence of pressures at the chordwise locations $x/D=\pm1.6$ for three spanwise distances ($\Delta z/D=0.42$, 1.0 and 2.08), according to the definition:

$$Coh(\Delta z,f)=\frac{|S(\Delta z,f)|}{\sqrt{S_{z=0}(f)S_{z=\Delta z}(f)}} \tag{3}$$

being $S(\Delta z,f)$ the cross spectrum and $S_{z=0}(f)$ and $S_{z=\Delta z}(f)$ the power spectra of surface pressures. Despite the numerical signal (computation with $L/B=2.0$) is not long enough to obtain a well defined function and apart from the evident difference in the Strouhal number (see Table 1), the comparison with the experimental data of Matsumoto et al. (2003) highlights that the numerical results overestimate the coherence of the pressure fluctuations at frequencies higher than the vortex shedding one at the upstream location $x/D=-1.6$. In contrast, at $x/D=1.6$ the coherence seems to be overestimated both at frequencies higher and lower than the Strouhal one.

5.3. Influence of the artificial dissipation

Despite the reasonable accuracy of the computed integral quantities, the resolution of turbulence in the DES computations previously described was not satisfying with respect to the mesh quality and time-step size. This is evident in Fig. 9 (top-right frame) where instantaneous scaled vorticity magnitude isocontours relative to the midspan plane are shown. Although an obvious improvement with respect to the URANS-LEA result (Fig. 9, top-left frame) is apparent, the numerical dissipation

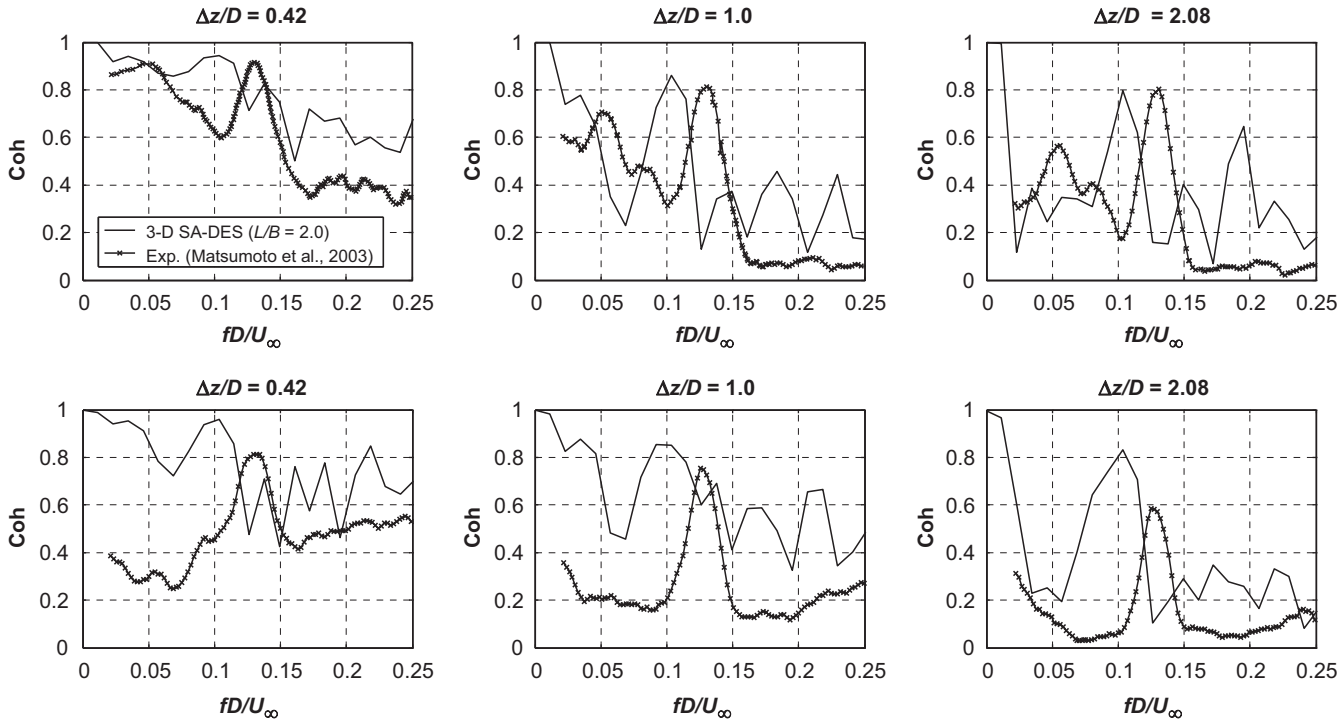

Fig. 8. Spanwise coherence of pressures. The top row corresponds to the upstream chordwise location ($x/D=-1.6$), while the bottom row to the downstream chordwise location ($x/D=1.6$). The numerical results refer to the case $L/B=2.0$ (2668 data sampled every $10\Delta t^*=0.17$). Experimental results from Matsumoto et al. (2003) refer to a Reynolds number of 40,000.

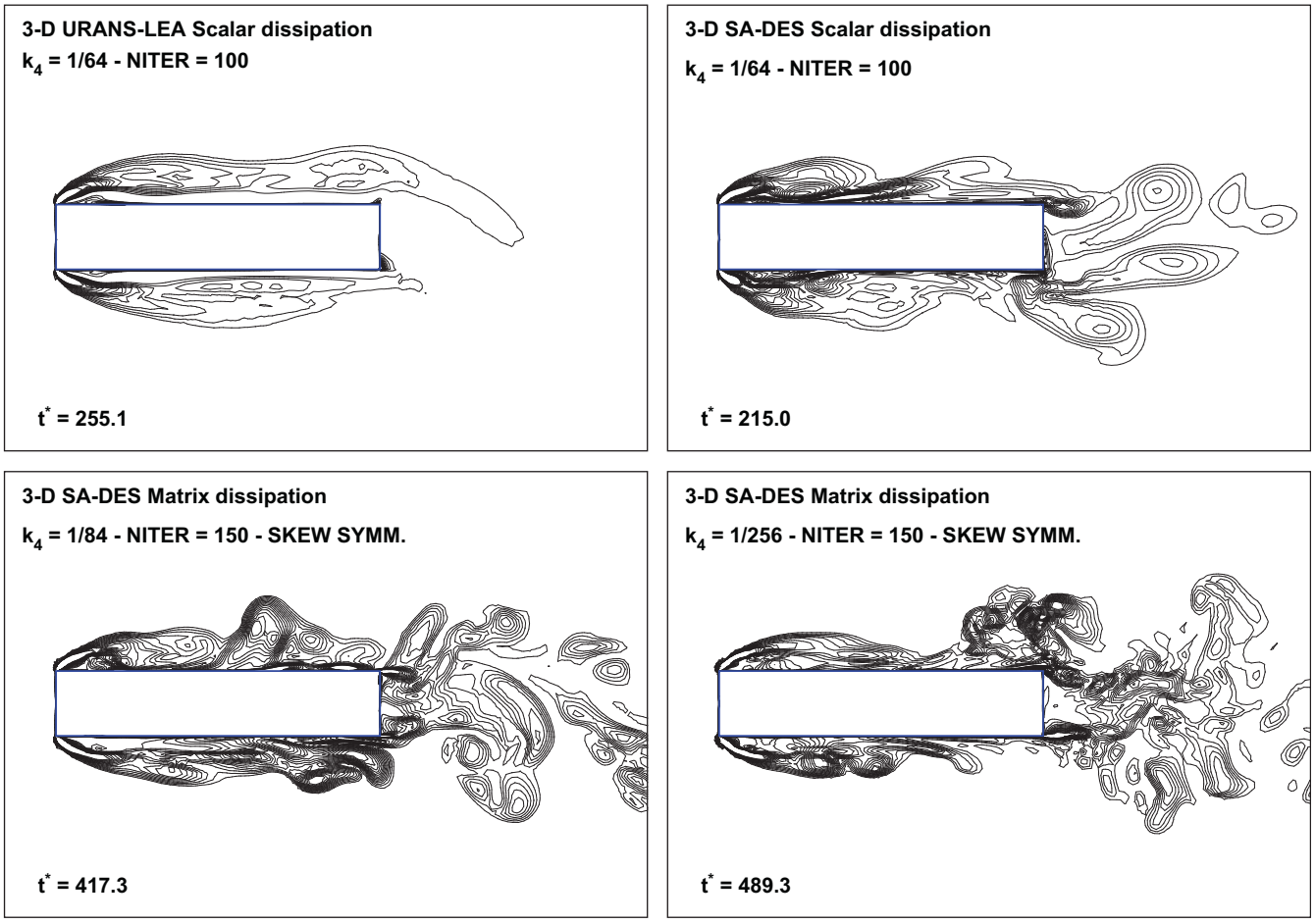

Fig. 9. Vorticity magnitude isocontours (scaled with B/U_∞; 14 levels from 7.5 to 40) relative to the midspan plane ($z/B=0.5$) for several computations ($L/B=1.0$).

seems to be able to damp out the high-wavenumber turbulent structures.

For this reason a series of additional computations were performed with the aim of reducing the artificial viscosity of the central difference numerical scheme. As discussed in Section 3.3, this can be done by adopting the matrix dissipation form of the algorithm instead of the scalar one. In addition, lower values of the fourth-order dissipation coefficient were tested, namely k_4 was first reduced from 1/64 to 1/84 (standard values recommended for the code used) and then a computation with $k_4=1/256$ was also performed. Much smaller values of this coefficient, such as $k_4=1/1000$, made the computation unstable. Furthermore, along with the divergence form of the inviscid fluxes, the skew-symmetric form was employed too, in order to minimize the aliasing errors. The number of inner iterations was increased from 100 to 150 to reduce the residuals that decrease slowly due to the stiffness of the compressible equations at low Mach number. In fact, as previously observed, the satisfaction of the continuity equation is a particularly important issue when the skew-symmetric operator is used. The DDES method (Spalart et al., 2006) was employed and the C_{DES} constant was increased to 0.65, due to the reduced numerical diffusion of the matrix dissipation form of the central difference scheme. In this way the LES mode was active in more than 82% of the volumes. In order to limit the computational burden, the mesh with a spanwise period equal to the cylinder chord was employed. The computations were restarted from the flow field previously computed with the scalar dissipation algorithm. Several attempts to further reduce the numerical dissipation through low-Mach number preconditioning (Choi and Merkle, 1993; Melberg and Heinrich, 2004) were also performed but without success in the case considered.

In terms of turbulence resolution the key role played by the amount of artificial viscosity introduced in the computation is evident from the analysis of Fig. 9. By using the matrix dissipation scheme finer vortical structures can be resolved and the full potential offered by the chosen computational grid and time-step size seems to be better exploited. The effect of reducing the fourth-order dissipation coefficient is also evident in Fig. 10 which shows an isosurface of the second invariant Q of the velocity gradient tensor, that for incompressible flows can be expressed as follows:

$$Q=\frac{1}{2}\sum_{i,\,j=1}^{3}(\Omega_{ij}\Omega_{ij}-S_{ij}S_{ij}) \tag{4}$$

where Ω and S are, respectively, the vorticity and the strain-rate tensors.

A comparison between the new computations performed is also possible through the lift coefficient time histories in Fig. 11 or in terms of integral quantities in Table 3. By using matrix dissipation the high-frequency content of the force coefficient signals increases. A significant reduction of the standard deviation of the lift and drag fluctuations is apparent. Also, for the cases with $k_4=1/84$ the mean drag slightly decreases and the Strouhal number increases. Concerning the effect of the number of inner iterations per physical time step, it seems that the standard-deviation values of lift and drag slightly decrease when 150 sub-iterations are performed, which highlights the importance of conveniently reducing the residuals also when the divergence form of the inviscid flux operator is used. Though the role of aliasing errors was supposed to be marginal with respect to truncation errors for second-order accurate solvers, the difference in terms of force coefficient fluctuations and Strouhal number does not seem completely negligible between the computations with divergence and skew-symmetric inviscid flux operators. Interestingly, a significantly lower Strouhal number, a slightly higher mean drag coefficient and a dramatic reduction of the lift fluctuations are observed in the case of the computation with lower fourth-order artificial viscosity ($k_4=1/256$), suggesting a drastic change in the flow topology. In fact, in Fig. 12 the time-averaged flow field is reported for both the computations with $k_4=1/84$ and $k_4=1/256$. If we compare the results with that of Fig. 4 for the basic case of scalar dissipation, it is apparent in the case with $k_4=1/84$ that the shear-layer mean reattachment point has non-negligibly moved upstream ($x/D=1.69$). In the case with $k_4=1/256$ the length of the mean recirculation bubble has become so small to be definitely incompatible with the pressure measurements available for Reynolds numbers similar to the one considered (Fig. 3). This fact underlines the sensitivity of the numerical results to the amount of artificial viscosity introduced in the solution through the discretization of the inviscid fluxes. Moreover, it is apparent that significant differences in the mean reattachment location produce variations in the mean drag coefficient and in the Strouhal number of few percents, whilst much more evident is their effect on the standard-deviation value of the lift coefficient.

6. Concluding remarks

It was shown that with the DES approach and a carefully designed three-dimensional grid fairly accurate results can be obtained for the benchmark test case of the 5:1 rectangular

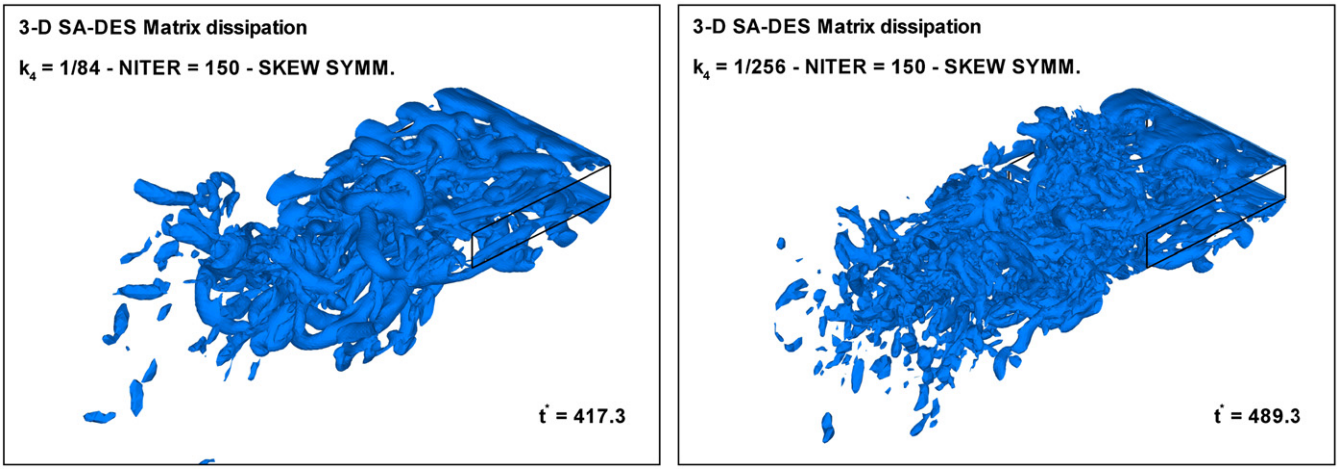

Fig. 10. Snapshots of the Q-invariant isosurface ($Q=50$) for two different levels of artificial dissipation ($k_4=1/84$ and 1/256).

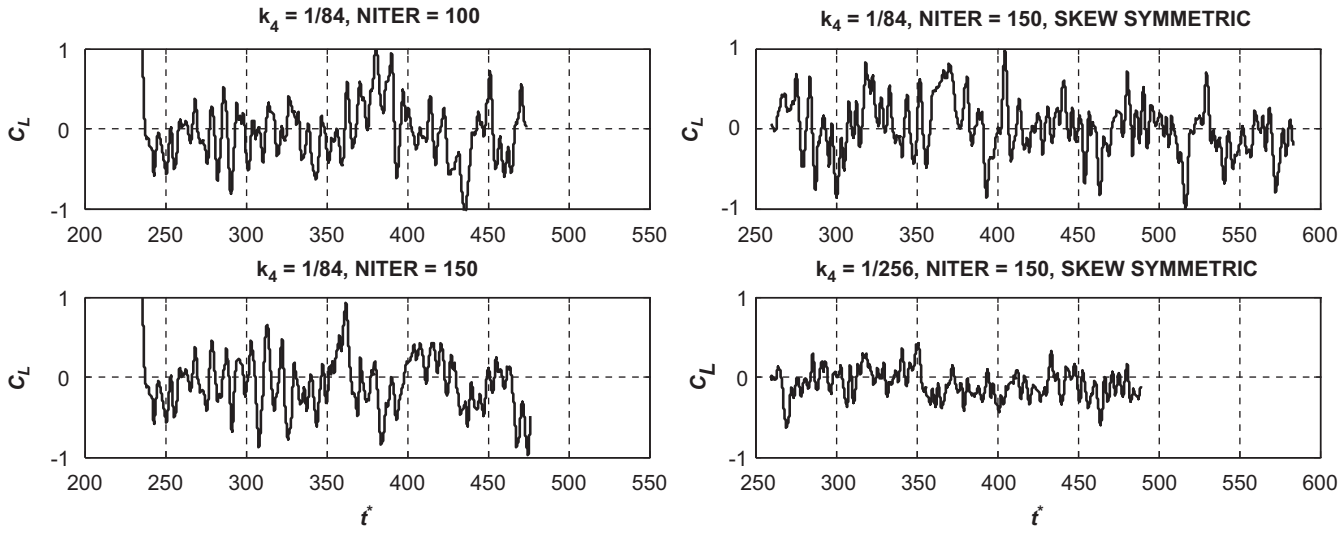

Fig. 11. Lift coefficient time histories computed with matrix dissipation schemes (divergence and skew-symmetric forms) and different values of the fourth-order artificial viscosity coefficient (k_4) and number of inner iterations (NITER) per physical time step ($L/B=1.0$).

Table 3
Strouhal number and mean (C_D, C_L) and standard-deviation (C_D', C_L') values of drag and lift coefficients computed with several central-difference schemes, different values of the fourth-order artificial viscosity coefficient (k_4) and number of inner iterations per physical time step (NITER). t^*_{INT} denotes the nondimensional time units considered for the calculation of the statistics ($L/B=1.0$).

Dissip.	Inviscid flux	k_4	C_{DES}	NITER	St	C_L	C_D	C_L'	C_D'	t^*_{INT}
Scalar	Divergence	1/64	0.45	100	0.103	0.047	1.016	0.553	0.055	464.5
Matrix	Divergence	1/84	0.65	100	0.118	−0.053	0.971	0.356	0.042	227.9
Matrix	Divergence	1/84	0.65	150	0.119	−0.087	0.967	0.333	0.035	225.6
Matrix	Skew symm.	1/84	0.65	150	0.114	−0.001	0.965	0.343	0.037	308.3
Matrix	Skew symm.	1/256	0.65	150	0.087	−0.085	0.998	0.173	0.030	213.3
Experiments (Schewe, 2009)					0.111	0.0	1.029	∼0.4		

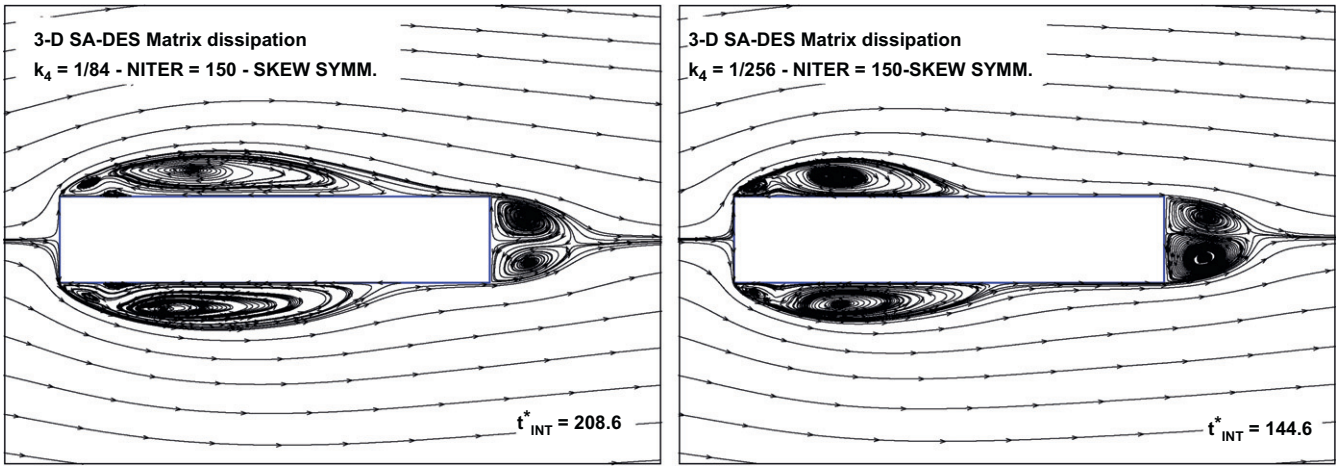

Fig. 12. Streamlines of the time-averaged flow field in case of matrix dissipation with two different values of the k_4 coefficient.

cylinder. In particular, the quality of the simulation is improved with respect to 2-D and 3-D URANS methods. Nevertheless, requirements of fine three-dimensional meshes, small time steps and reasonable statistical convergence of the computed flow field make this approach quite expensive for the simulation of bluff body flows.

The cost of the computation is tightly related also to the choice of the spanwise period of the computational domain and in the present work it was shown that one-chord length might be not enough to allow the free development of three-dimensional large-scale flow structures. A clear improvement was obtained by doubling the spanwise period but this is probably still not sufficient to completely remove the effect of periodic boundary conditions imposed at the lateral planes of the computational domain.

The key role played by the artificial viscosity introduced in the computation through the discretization of the inviscid fluxes was also highlighted. In particular, it was pointed out that the

resolution of small-scale turbulent structures can be improved and obviously this has significant effects on the mechanism of shedding of large-scale eddies and therefore on integral quantities of practical engineering interest, such as the aerodynamic force coefficients. As the use of the LES and DES approach in combination with unstructured meshes and second-order accurate algorithms is nowadays fairly common in the computational wind engineering community, the development of convenient strategies of reduction of the numerical dissipation, while keeping stable the computation and avoiding spurious oscillations in the solution, is an important research direction in this field.

Finally, the good results obtained with DES for the BARC case study, employing hybrid meshes and an unstructured solver, are promising in view of the challenge offered by detailed engineering structure aerodynamics and fluid–structure coupling problems at high Reynolds numbers in the case of geometries with significant rounded surfaces, where the cost of a well-resolved LES may be prohibitive. On the other hand, the sensitivity of the results to the numerical scheme adopted for the discretization of the inviscid fluxes or to the spanwise extension of the computational domain makes clear the point that state-of-the-art CFD simulations are still far from being alternative to experiments for bluff body flows. Nevertheless, numerical analyses can be a powerful complement to wind tunnel tests, in particular in order to explain experimental evidences, the physical origin of which is not clear, as shown for instance in Mannini et al. (2010a,b).

Acknowledgements

This work has been performed in the framework of the DLR projects "Numerische Simulation der Umströmung stumpfer Körper" (2007–2008) and "3D-Effekte bei abgelösten Strömungen" (2009–2011). The support received is gratefully acknowledged. Dr. Ralph Voβ, from the Institute of Aeroelasticity, and Dr. Tobias Knopp and Dr. Keith Weinman, from the Institute of Aerodynamics and Flow Technology of DLR Göttingen, are also thanked for their suggestions and the helpful discussions. The help of Urte Fürst in using the computer cluster of the DLR Institute of Aeroelasticity is also gratefully acknowledged. Finally the authors would like to thank Prof. Masaru Matsumoto, from Kyoto University, for the experimental data he kindly made available.

References

Bartoli, G., Bruno, L., Buresti, G., Ricciardelli, F., Salvetti, M.V., Zasso, A., 2008. BARC overview document. 〈http://www.aniv-iawe.org/barc〉.

Bartoli, G., Righi, M., 2006. Flutter mechanism for rectangular prisms in smooth and turbulent flow. J. Wind Eng. Ind. Aerodyn. 94 (5), 275–291.

Berrone, S., Garbero, V., Marro, M., 2010. Numerical simulation of incompressible flows past a rectangular cylinder based on adaptive finite element and finite volume methods. In: Proceedings of the Fifth International Symposium on Computational Wind Engineering, Chapel Hill, North Carolina, USA.

Bruno, L., Fransos, D., Coste, N., Bosco, A., 2010. 3D flow around a rectangular cylinder: a computational study. J. Wind Eng. Ind. Aerodyn. 98 (6–7), 263–276.

Choi, Y.-H., Merkle, C.L., 1993. The application of preconditioning in viscous flows. J. Comput. Phys. 105 (2), 207–223.

Collie, S., Gerritsen, M., Jackson, P., 2008. Performance of two-equation turbulence models for flat plate flows with leading edge bubbles. J. Fluids Eng. 130 (2), 1–11, 021201.

Crompton, M.J., 2001. The thin aerofoil leading edge bubble. Ph.D. Thesis, University of Bristol, UK.

Ducros, F., Laporte, F., Soulères, T., Guinot, V., Moinat, P., Caruelle, B., 2000. High-order fluxes for conservative skew-symmetric-like schemes in structured meshes: application to compressible flows. J. Comput. Phys. 161 (1), 114–139.

Edwards, J.R., Chandra, S., 1996. Comparison of eddy viscosity-transport turbulence models for three-dimensional, shock-separated flowfields. Am. Inst. Aeronaut. Astronaut. J. 34 (4), 756–763.

Galli, F., 2005. Comportamento aerodinamico di strutture snelle non profilate: approccio sperimentale e computazionale. Master's Thesis, Politecnico di Torino, Turin, Italy (in Italian).

Gerhold, T., Galle, M., Friedrich, O., Evans, J., 1997. Calculation of complex three-dimensional configurations employing the DLR-Tau code. In: Proceedings of the 35th AIAA Aerospace Sciences Meeting and Exhibit, Reno, Nevada, USA, AIAA Paper 97-0167.

Haase, W., Aupoix, B., Bunge, U., Schwamborn, D., 2006. Flomania—a European initiative on flow physics modelling. Notes on Numerical Fluid Mechanics and Multidisciplinary Design, vol. 94. Springer, Berlin, Heidelberg, New York.

Hansen, R.P., Forsythe, J.R., 2003. Large and Detached Eddy Simulations of a circular cylinder using unstructured grids. In: Proceedings of the 41st AIAA Aerospace Sciences Meeting and Exhibit, Reno, Nevada, USA, AIAA Paper 2003-0775.

Jameson, A., Schmidt, W., Turkel, E., 1981. Numerical solutions of the Euler equations by finite volume methods using Runge–Kutta time stepping. In: Proceedings of the 19th AIAA Aerospace Sciences Meeting and Exhibit, Reno, Nevada, USA, AIAA Paper 81-1250.

Knisely, C.W., 1990. Strouhal numbers of rectangular cylinders at incidence: a review and new data. J. Fluids Struct. 4 (4), 371–393.

Kravchenko, A.G., Moin, P., 1997. On the effect of numerical errors in Large Eddy Simulations of turbulent flows. J. Comput. Phys. 131 (2), 310–322.

Lübcke, H., Schmidt, S., Rung, T., Thiele, F., 2001. Comparison of LES and RANS in bluff-body flows. J. Wind Eng. Ind. Aerodyn. 89 (14–15), 1471–1485.

Mannini, C., Šoda, A., Voß, R., Schewe, G., 2007. URANS and DES simulation of flow around a rectangular cylinder. In: Tropea, C., Jakirlic, S., Heinemann, H.-J., Henke, R., Hönlinger, H. (Eds.), Notes on Numerical Fluid Mechanics and Multidisciplinary Design, vol. 96, Proceedings of the 15th DGLR-Fach-Symposium der STAB, Darmstadt, Germany, 2006. Springer, Berlin, Heidelberg, New York, pp. 36–43.

Mannini, C., Šoda, A., Schewe, G., Weinman, K., 2008. Detached-Eddy Simulation of flow around a 1:5 rectangular cylinder. In: Belloli, M., Cheli, F., Diana, G., Muggiasca, S., Rocchi, D., Zasso, A. (Eds.), Proceedings of the Sixth International Colloquium on Bluff Body Aerodynamics and Applications, Milan, Italy.

Mannini, C., Weinman, K., Šoda, A., Schewe, G., 2009. Three-dimensional numerical simulation of flow around a 1:5 rectangular cylinder. In: Borri, C., Augusti, G., Bartoli, G., Facchini, L. (Eds.), Proceedings of the Fifth European and African Conference on Wind Engineering. Firenze University Press, Florence, Italy.

Mannini, C., Šoda, A., Schewe, G., 2010a. Unsteady RANS modelling of flow past a rectangular cylinder: investigation of Reynolds number effects. Comput. Fluids 39 (9), 1609–1624.

Mannini, C., Šoda, A., Voß, R., Schewe, G., 2010b. Unsteady RANS simulations of flow around a bridge section. J. Wind Eng. Ind. Aerodyn. 98 (12), 742–753.

Matsumoto, M., 1996. Aerodynamic damping of prisms. J. Wind Eng. Ind. Aerodyn. 59 (2–3), 159–175.

Matsumoto, M., 2005. Personal communication.

Matsumoto, M., Shirato, H., Araki, K., Haramura, T., Hashimoto, T., 2003. Spanwise coherence characteristics of surface pressure field on 2-D bluff bodies. J. Wind Eng. Ind. Aerodyn. 91 (1–2), 155–163.

Mavriplis, D.J., Jameson, A., Martinelli, L., 1989. Multigrid solution of the Navier–Stokes equations on triangular meshes. In: Proceedings of the 27th AIAA Aerospace Sciences Meeting, AIAA Paper 89-0120, Reno, Nevada, USA.

Melber, S., Heinrich, R., 2004. Low Mach-number preconditioning for the DLR-TAU code and application to high-lift flows. In: Breitsamter, C., Laschka, B., Heinemann, H.J., Hilbig, R. (Eds.), Notes on Numerical Fluid Mechanics and Multidisciplinary Design, vol. 87, New Results in Numerical and Experimental Fluid Mechanics IV. Springer, Berlin, Heidelberg, New York, pp. 390–397.

Mills, R., Sheridan, J., Hourigan, K., 2002. Response of base suction and vortex shedding from rectangular prisms to transverse forcing. J. Fluid Mech. 461, 25–49.

Nakamura, Y., Mizota, T., 1975. Torsional flutter of rectangular prisms. J. Eng. Mech. Div. 101 (EM2), 125–142.

Nakamura, Y., Nakashima, M., 1986. Vortex excitation of prisms with elongated rectangular, H and ⊢ cross-sections. J. Fluid Mech. 163, 149–169.

Nakamura, Y., Ohya, Y., Tsuruta, H., 1991. Experiments on vortex shedding from flat plates with square leading and trailing edges. J. Fluid Mech. 222, 437–447.

Nakamura, Y., Yoshimura, T., 1982. Flutter and vortex excitation of rectangular prisms in pure torsion in smooth and turbulent flows. J. Sound Vib. 84 (3), 305–317.

Okajima, A., 1982. Strouhal numbers of rectangular cylinders. J. Fluid Mech. 123, 379–398.

O'Neill, P.L., Nicolaides, D., Honnery, D., Soria, G., 2004. Autocorrelation functions and the determination of integral length with reference to experimental and numerical data. In: Proceedings of the 15th Australasian Fluid Mechanics Conference, Sydney, Australia.

Parker, R., Welsh, M.C., 1983. Effects of sound on flow separation from blunt flat plates. Int. J. Heat Fluid Flow 4 (2), 113–127.

Ricciardelli, F., 2010. Effects of the vibration regime on the spanwise correlation of the aerodynamic forces on a 5:1 rectangular cylinder. J. Wind Eng. Ind. Aerodyn. 98 (4–5), 215–225.

Ricciardelli, F., Marra, A.M., 2008. Sectional aerodynamic forces and their longitudinal correlation on a vibrating 5:1 rectangular cylinder. In: Belloli, M., Cheli, F., Diana, G., Muggiasca, S., Rocchi, D., Zasso, A. (Eds.), Proceedings of the Sixth International Colloquium on Bluff Body Aerodynamics and Applications, Milan, Italy.

Rung, T., Lübcke, H., Franke, M., Xue, L., Thiele, F., Fu, S., 1999. Assessment of explicit algebraic stress models in transonic flows. In: Rodi, W., Laurence, D. (Eds.), Proceedings of the Fourth International Symposium on Engineering Turbulence Modelling and Experiments, Ajaccio, France. Elsevier, Amsterdam, pp. 659–668.

Schewe, G., 2006. Influence of the Reynolds-number on flow-induced vibrations of generic bridge sections. In: Radić J. (Ed.), Proceedings of the International Conference on Bridges, Dubrovnik, Croatia, pp. 351–358.

Schewe, G., 2009. Reynolds-number-effects in flow around a rectangular cylinder with aspect ratio 1:5. In: Borri, C., Augusti, G., Bartoli, G., Facchini, L. (Eds.), Proceedings of the Fifth European and African Conference on Wind Engineering. Firenze University Press, Florence, Italy.

Schewe, G., Larsen, A., 1998. Reynolds number effects in the flow around a bluff bridge deck cross section. J. Wind Eng. Ind. Aerodyn. 74–76, 829–838.

Schwamborn, D., Gerhold, T., Kessler, K., 1999. DLR-TAU code—an overview. In: Proceedings of the First ONERA/DLR Aerospace Symposium, Paris, France.

Shimada, K., Ishihara, T., 2002. Application of a modified k–ε model to the prediction of aerodynamic characteristics of rectangular cross-section cylinders. J. Fluids Struct. 16 (4), 465–485.

Shur, M.L., Spalart, P.R., Squires, K.D., Strelets, M.Kh., Travin, A.K., 2005. Three dimensionality in Reynolds-averaged Navier–Stokes solutions around two-dimensional geometries. Am. Inst. Aeronaut. Astronaut. J. 43 (6), 1230–1242.

Shur, M.L., Spalart, P.R., Strelets, M.Kh., Travin, A.K., 1999. Detached-eddy simulation of an airfoil at high angle of attack. In: Rodi, W., Laurence, D. (Eds.), Proceedings of the Fourth International Symposium on Engineering Turbulence Modelling and Experiments, Ajaccio, France. Elsevier, Amsterdam, pp. 669–678.

Šoda, A., 2006. Numerical investigation of unsteady transonic shock/boundary-layer interaction for aeronautical applications. Ph.D. Thesis, RWTH Aachen, Germany.

Spalart, P.R., 2000. Strategies for turbulence modelling and simulations. Int. J. Heat Fluid Flow 21 (3), 252–263.

Spalart, P.R., 2001. Young–Person's guide to Detached-Eddy Simulation grids. NASA CR-2001-211032.

Spalart, P.R., Allmaras, S.R., 1992. A one-equation turbulence model for aerodynamic flows. In: Proceedings of the 30th AIAA Aerospace Sciences Meeting and Exhibit, AIAA Paper 1992-0439, Reno, Nevada, USA.

Spalart, P.R., Deck, S., Shur, M.L., Squires, K.D., Strelets, M.Kh., Travin, A.K., 2006. A new version of Detached-Eddy Simulation, resistant to ambiguous grid densities. Theor. Comput. Fluid Dyn. 20 (3), 181–195.

Spalart, P.R., Jou, W.-H., Strelets, M.Kh., Allmaras, S.R., 1997. Comments on the feasibility of LES for wings, and on a hybrid RANS/LES approach. In: Liu, C., Liu, Z. (Eds.), Advances in DNS/LES, Proceedings of the First AFOSR International Conference on DNS/LES, Ruston, Louisiana, USA, Greyden Press, Columbus, Ohio, pp. 137–147.

Stokes, A.N., Welsh, M.C., 1986. Flow-resonant sound interaction in a duct containing a plate, II: square leading edge. J. Sound Vib. 104 (1), 55–73.

Strelets, M.Kh., 2001. Detached Eddy Simulation of massively separated flows. In: Proceedings of the 39th AIAA Aerospace Sciences Meeting and Exhibit, Reno, Nevada, USA, AIAA Paper 2001-0879.

Swanson, R.C., Turkel, E., 1992. On central-difference and upwind schemes. J. Comput. Phys. 101 (2), 292–306.

Tamura, T., Ito, Y., 1996. Aerodynamic characteristics and flow structures around a rectangular cylinder with a section of various depth/breadth ratios. J. Struct. Constr. Eng. (Trans. Architect. Inst. Jpn.) 486, 153–162 (in Japanese).

Travin, A.K., Shur, M.L., Strelets, M.Kh., Spalart, P.R., 1999. Detached-eddy simulations past a circular cylinder. Flow Turbul. Combust. 63 (1–4), 293–313.

Turkel, E., 1988. Improving the accuracy of central difference schemes. ICASE Report No. 88-53. NASA, Langley Research Center, Hampton, Virginia, USA.

Weinman, K., van der Ven, H., Mockett, C., Knopp, T., Kok, J., Perrin, R., Thiele, F., 2006. A study of grid convergence issues for the simulation of the massively separated flow around a stalled airfoil using DES and related methods. In: Wesseling, P., Oñate, E., Périaux, J. (Eds.), Proceedings of the European Conference on Computational Fluid Dynamics, Egmond aan Zee, The Netherlands.

Whitfield, D.L., Janus, J.M., 1984. Three-dimensional unsteady Euler equations solution using flux vector splitting. In: Proceedings of the 17th AIAA Fluid Dynamics, Plasma Dynamics and Lasers Conference, Snowmass, Colorado, USA, AIAA Paper 84-1552.

Wilcox, D.C., 1988. Reassessment of the scale-determining equation for advanced turbulence models. Am. Inst. Aeronaut. Astronaut. J. 26 (11), 1299–1310.

Wilcox, D.C., 2006. Turbulence Modelling for CFD, Third ed. DCW Industries, Inc., La Cañada, California, USA.